J. Plasma Physics (1999), *vol.* 61, *part* 1, *pp.* 43–50. Printed in the United Kingdom

Analysis of rippled shock-wave propagation and ablation-front stability by theory and hydrodynamic simulation

N. MATSUI, K. MIMA, M. HONDA and A. NISHIGUCHI*

Institute of Laser Engineering, Osaka University, 2–6 Yamada-Oka, Suita, Osaka, 565-0871 Japan

(Received 27 January 1998 and in revised form 24 June 1998)

The hydrodynamic start-up problem is one of the most crucial issues in laser-driven symmetrical implosion. The target-surface roughness and initial imprint by nonuniform laser irradiation result in Rayleigh–Taylor instability in the acceleration and deceleration phase. To estimate the tolerance of the target-surface roughness, the temporal behaviour of corrugated ablation surface and rippled shock-wave propagation are investigated using a perturbation analysis of the fluid equation, which is solved under the boundary model of a fire-polished ablation surface. The results show good agreement with two-dimensional hydrodynamic simulation and experimental results [T. Endo et al., *Phys. Rev. Lett.* **74**, 3608 (1995)].

1. Introduction

In laser-driven symmetrical implosion, the target-surface roughness and nonuniform laser irradiation cause hydrodynamic instabilities: Richtmyer–Meshkov instability (Richtmyer 1960; Meshkov 1969), Rayleigh–Taylor (RT) instability (Chandrasekhar 1961), and so forth. These instabilities degrade the symmetrical performance of the imploding shell. Namely, RT instability in the acceleration phase and the following feedthrough result in RT in the deceleration phase, which implies that fuel-pusher mixing causes a significant reduction in the spark temperature. Therefore it is necessary to estimate the tolerance of the roughness of the target surface and the nonuniformity of the irradiating laser beam. When a laser beam illuminates a corrugated target surface uniformly, a rippled strong shock wave, whose front shape is the same as the initial corrugated target surface, is launched immediately, and the strong shock-wave front oscillates and propagates, passing through the target. The oscillation period is approximately the perturbation wavelength. Although the propagation of a corrugated shock wave and the following RM instabilities appear in many aspects of laser-driven implosion, little work has been done so far to study the behaviour of the nonuniformly compressed fluid.

The first analysis of corrugated shock-wave propagation was performed by Richtmyer (1960). Briscoe and Kovitz (1968) explained that the shock-wave shape is described by Bessel functions. Munro (1989) investigated rippled-

* Present address: Osaka Institute of Technology, Omiya Asahi-ku, Osaka, 535 Japan.

shock propagation analytically, and the analytical solutions serve as useful test problems for the complex hydrodynamic code for inertial fusion. Ishizaki et al. (1996) studied the instability of a contact surface driven by a rippled shock wave. Rutkevich et al. (1996) found that the spontaneous emission of sound waves from strong shocks in metals results in corrugation of a planar shock front. Recently, analytical models have been obtained for the RM instability in the linear regime (Wouchuk and Nishihara 1996, 1997) and the propagation of the rippled shock wave driven by nonuniform laser ablation (Ishizaki and Nishihara 1997). Experimental results on the growth of the rippled shock and the areal mass density perturbation have been presented by Endo et al. (1995).

In this paper, the Euler equation of an ideal fluid is solved by linear analysis with given boundary conditions at the ablation front, where we take account of the fire-polishing effects due to lateral heat conduction. The results are compared with the numerical-simulation results. We have used the two-dimensional fluid particle-in-cell (PIC) simulation code (IZANAMI) (Nishiguchi and Yabe 1983), which includes the various physical processes: hot electron transport, radiation and radiative transfer, laser absorption, and so on.

This paper is organized as follows. In Sec. 2 the basic equations are described, and boundary conditions on both the ablation front and the shock front are specified. Note that this linear analysis is characterized by the boundary condition on the ablation front. Analytical results are given in Sec. 3. The dependences of the rippled shock-front oscillation on a free parameter α and the specific-heat ratio γ are discussed. The physical meaning of the parameter α will be introduced later. The behaviour of the ablation front is also presented. Section 4 is devoted to a comparison between the analytical results and the simulation results using the IZANAMI code. As an extension of this work, the analytical results are also compared with the experimental results. Finally, Sec. 5 contains concluding remarks.

2. Linear theoretical analysis

Let us consider the case when a rippled shock is driven by a nonuniform piston and propagates in a uniform solid target. As shown in Fig. 1, the piston and the initial shock front have a sinusoidal distortion of wavelength λ. The perturbation amplitude is assumed to be small, so that the fluid equations can be linearized (Munro 1989). For the boundary conditions on the nonuniform piston, namely the ablation front, we assume that the pressure perturbation has the opposite phase to the perturbation amplitude on the ablation front. Other boundary conditions at the shock front are given by the jump conditions across the shock front. Using the fourth-order Runge–Kutta method, we have solved the linearized fluid equations with the above-mentioned boundary conditions in the moving frame of the ablation front.

2.1. Basic equations

We begin with the Euler equation of an ideal fluid. By Fourier-decomposing for the lateral component of the fluid perturbation, for example $P(x, y, t) = p(x, t) \exp(iky)$ and eliminating the velocity and density fluctuations in the linearized Euler equation, we arrive straightforwardly at the sound-wave equation

https://doi.org/10.1017/S0022377898007260 Published online by Cambridge University Press

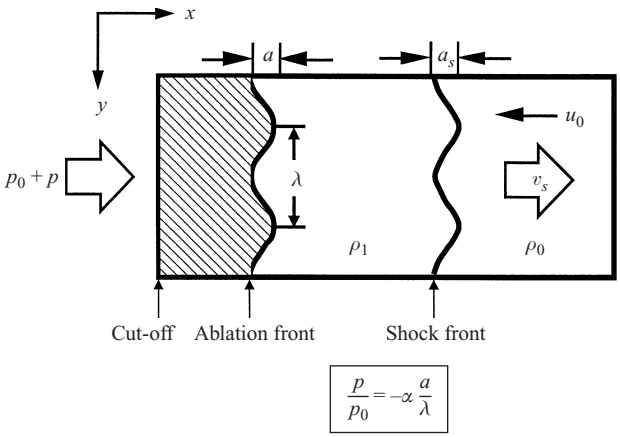

Figure 1. Schematic view of the whole analytical and simulation system. Note that the physical meaning of the free parameter α is that it represents the phenomenological fire-polishing effects on that ablation front (see text).

propagating along the x direction in the form of the Klein–Gordon equation as follows:

$$\frac{\partial^2 p(x,t)}{\partial t^2} = c^2 \frac{\partial^2 p(x,t)}{\partial x^2} - \kappa^2 c^2 p(x,t), \tag{1}$$

where $\kappa = 2\pi/\lambda$ is the wavenumber in the y direction, $p(x,t)$ is the pressure perturbation and c is the sound speed. The shock front propagates along the x direction. This equation is solved in the shock-compression region under the boundary conditions given below.

2.2. Boundary conditions on the ablation front

The condition that there is no mass ablation of first order on the ablation front yields $da/dt = u$, where $a(t) \equiv \xi(0,t)$ is the perturbed amplitude of the ablation front $x = 0$, and u is the perturbed velocity of the fluid on the ablation front. The pressure perturbation at the ablation front, $p_a(t) \equiv p(0,t)$, and the ablation-front ripple amplitude a are related by $p_a/p_0 = -\alpha(a/\lambda)$, where p_0 is the unperturbed pressure and $\alpha > 0$ is a free parameter. This relation means that the phase of the pressure perturbation is opposite to that of the ablation-front ripple. The physical mechanism of this relation can be explained as follows. As shown in Fig. 1, the cut-off surface where the laser deposits the energy is approximately flat even if the ablation front is rippled, since thermal conduction and hydrodynamic motion smooth out the nonuniformity of the ablation plasma. As can be expected from Fig. 1, the tops of the ripples are closer to the cut-off surface than the bottoms of the ripples. This means that the heat flux at the tops of the ripples is higher than that at the bottoms. Therefore the pressure at the tops of the spikes on the ablation front is higher than that at the bottoms of the bubbles. This will suppress the growth of perturbations on the ablation front. Using the above relations, the equation of motion can be written in the form

$$\frac{\partial^2 p_a}{\partial t^2} = \frac{\alpha p_0}{\rho_1 \lambda} \left[\frac{\partial p}{\partial x} \right]_{x=0}, \tag{2}$$

https://doi.org/10.1017/S0022377898007260 Published online by Cambridge University Press

where ρ_1 is the compressed fluid density behind the shock front. Equation (2) is consistently used as the boundary condition for the ablation front. Note here that the ablation pressure in the stationary ablation is proportional to $q^{2/3}$ for the heat flux q at the ablation front and the fluctuation in q, δq, due to the surface ripple is proportional to a/d. Therefore we assume that the pressure perturbation is given by $\alpha a/\lambda$.

2.3. Boundary conditions on the shock front

From the shock Hugoniot relation of the first order, the amplitude of the ripple of the shock front $a_s(t) = \xi(v_s t, t)$ is given by

$$\frac{da_s(t)}{dt} = \frac{1}{2}\frac{1}{\rho_1 - \rho_0}\left(\frac{1}{v_s} - \frac{v_s}{c^2}\right) p(v_s t, t), \tag{3}$$

where ρ_0 is the fluid density ahead of the shock front and v_s is the shock velocity in the flame moving with the ablation front. In addition to (3), we assume that there is no perturbation ahead of the shock front and that the tangential velocity on both sides of the shock is continuous, to obtain

$$\frac{1}{2}\left(3v_s + \frac{c^2}{v_s}\right)\frac{dp(v_s t, t)}{dt} = (v_s^2 - c^2)\left[\frac{\partial p}{\partial x}\right]_{x = v_s t} + \kappa^2 c^2 u_0 \rho_1 v_s a_s(t), \tag{4}$$

where u_0 is the velocity of the ablation front in the laboratory frame. Note that (3) and (4) are identical to those for the isentropic case, (36) and (42) respectively in Richtmyer (1960). Now we can solve (1) by using the boundary conditions (2)–(4).

3. Analytical results

The results obtained by solving (1) are shown in Figs 2 and 3. Henceforth unless otherwise indicated, the parameters $\alpha = 2$, $\gamma = \frac{5}{3}$ and $\dot{m} = 1.7 \times 10^5$ g cm^2 s^{-1}, $\dot{a}(t = 0) = -1.6 \times 10^5$ cm s^{-1} are fixed, unless where γ is the specific-heat ratio and $\dot{m}$ is the zeroth-order mass ablation rate per unit area and unit time. Note that mass-ablation effects could be considered by replacing the ablation-front velocity u_0 by $u_0 = u_0 + \dot{m}/\rho_1$. The ablation effects on ripple-shock propagation are insignificant, since the condition $u_0 \gg \dot{m}/\rho_1$, is satisfied for typical target parameters and laser conditions. The analytical results show that the oscillation period of the shock front is only a few percent shorter than that obtained in the case of no mass ablation, because the bounce-back distance of a sound wave in the compressed region becomes slightly shorter. The initial amplitude of the rippled shock, $a_0 = \xi(0, 0)$, is 5.0 μm. The wavelength of the corrugated target surface $\lambda = 100\,\mu$m. Figures 2(a) and (b) indicate the dependences of the rippled shock growth on α and γ respectively. As mentioned above, the decaying oscillation of the shock-front ripple is shown in Fig. 2. The parameter α defines the ratio of the perturbed pressure to the ablation-front ripple amplitude, and is assumed to be constant in time. If we assume that $\alpha = 2$ then p_a/p_0 becomes 0.1 when $a/\lambda = 0.5$. The physical meaning will be clear if we define the boundary condition on the ablation front as $p_a/p_0 = -\alpha' a/d$ by introducing the distance d between the ablation front and the cut-off front (stand-off distance). For steady-state ablation, the heat-flux perturbation at

https://doi.org/10.1017/S0022377898007260 Published online by Cambridge University Press

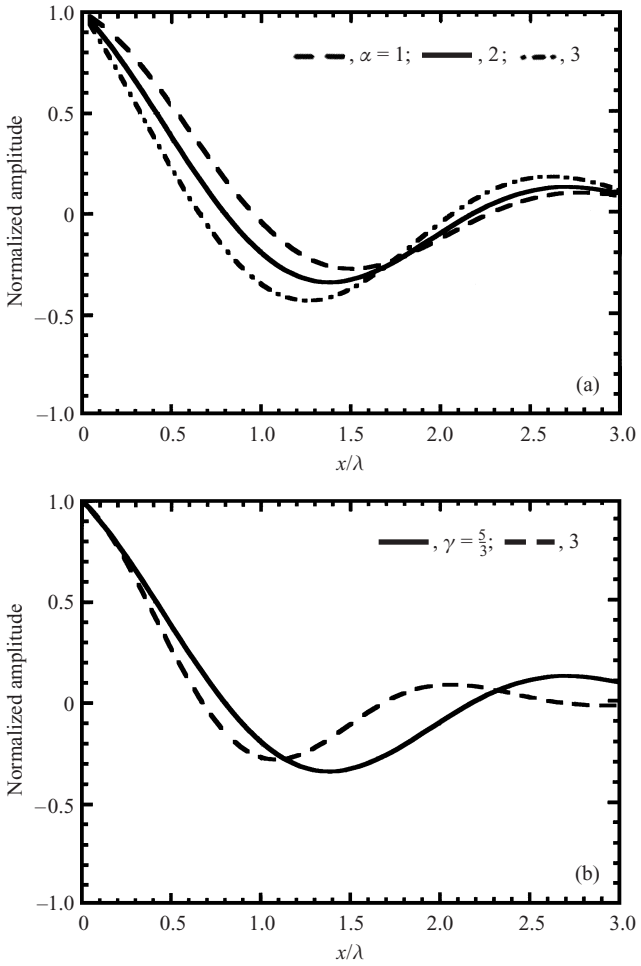

Figure 2. Amplitude of the shock-front ripple normalized by the initial amplitude versus the shock-wave propagation distance x. The temporal behaviour of the shock-front ripple depends on (a) the smoothing parameter α and (b) the specific-heat ratio γ.

the front, $\delta q/q_0 \approx -\frac{7}{5}a/d_0$ when the stand-off distance d is normalized by a. Since the ablation pressure is proportional to $q^{2/3}$, $p_a/p_0 = -\frac{14}{15}a/d_0$. That is, the parameter α' will be of order unity in general, and α is given by $\alpha'\lambda/d$. Usually, d is time-dependent in the simulation, and varies from 50 μm to 200 μm. In the steady-state theory, d is roughly scaled by $d \approx 360(\lambda_L/0.53\,\mu\text{m})^{14/3}(I_L/10^{14}\text{ W cm}^2)^{4/3}$ in μm, where λ_L and I_L are the laser wavelength and intensity respectively (Manheimer et al. 1982). The stand-off distance d, whose scaling law is derived from simple modelling of convective fluid and electron transport, tends to be short in the full hydrodynamic simulations. The parameter α', which includes all the other effects apart from the time–space scale universality of the Euler fluid (e.g. thermal smoothing due to coronal clouds, nonlocal transport of electron and radiation, and so on), should be determined by subsequent use of this analytical model.

As shown in Fig. 2(a), increasing the parameter α increases the value of p_a/p_0, so the oscillation period of the rippled shock becomes shorter and the maximum

https://doi.org/10.1017/S0022377898007260 Published online by Cambridge University Press

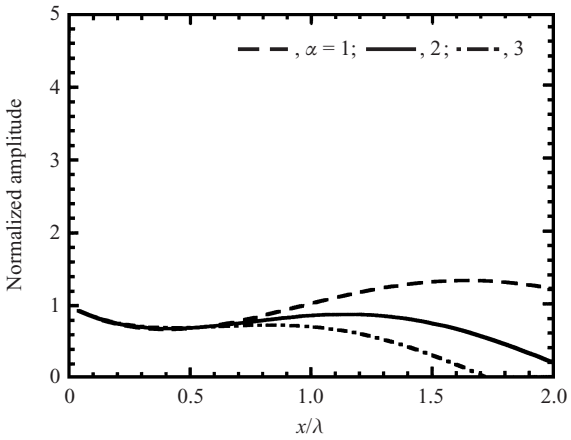

Figure 3. The α dependence of the amplitude of the ablation-front ripple normalized by the initial amplitude. The horizontal axis is the same as in Fig. 2.

amplitude of the shock-front ripple becomes larger, and the perturbation amplitude tends towards overshoot. The γ dependences are shown in Fig. 2(b). Larger γ implies a more-rigid material, and so makes the sound speed higher, and the oscillation period of the rippled shock becomes shorter. It should be noted that the polytropic index could also include a deviation from adiabatic compression. Figure 3 shows the α dependence of the temporal behaviour of the ablation-front ripple. It is found that the ablation-front ripple amplitude is almost constant in time. As expected, larger α suppresses the growth of the ablation front ripple more effectively.

4. Comparison of analytical results with simulation results

The rippled shock-wave problem has also been simulated using the two-dimensional hydrodynamic PIC code (IZANAMI). We have performed the simulation on the propagation of a rippled shock launched by uniform laser irradiation of a corrugated target surface. The initial target parameters and laser conditions for numerical simulations are as follows: the peak laser intensity is 10^{14} W cm^{-2}, with a rise time of 150 ps; the laser wavelength is 0.53 μm; the initial amplitude of the ablation-front ripple $a_0 = 5.0$ or 3.0 μm; the wavelength of the corrugated shockwave surface $\lambda = 100$ or 50 μm; the target thickness is about 110 μm. We choose $\gamma = \frac{5}{3}$ in this simulation. Note that d changes from 50 μm to 200 μm in the simulation; that is, α changes from 2 to 0.5 for $\alpha' = 1$ and $\lambda = 100$ μm. We compare the simulation results with those of the linear analysis in the case of $\alpha = 2$. Figures 4(a) and (b) show the temporal behaviours of the amplitudes of the shock-front and ablation-front ripples respectively. The behaviour of the rippled shock in the simulation is very similar to that of the linear analysis, as shown in Fig. 4(a). The period and the maximum amplitude of the ripple are almost the same in both cases. The fact that there is a possibility of a short period for a large polytrope index γ as shown in Fig. 2(b) might lead one to think that the difference between the analytical and simulation results in Fig. 4(a) could be attributed to the incorrect prediction of dissipative effects. Meanwhile, Fig. 4(b) shows that the simulation

https://doi.org/10.1017/S0022377898007260 Published online by Cambridge University Press

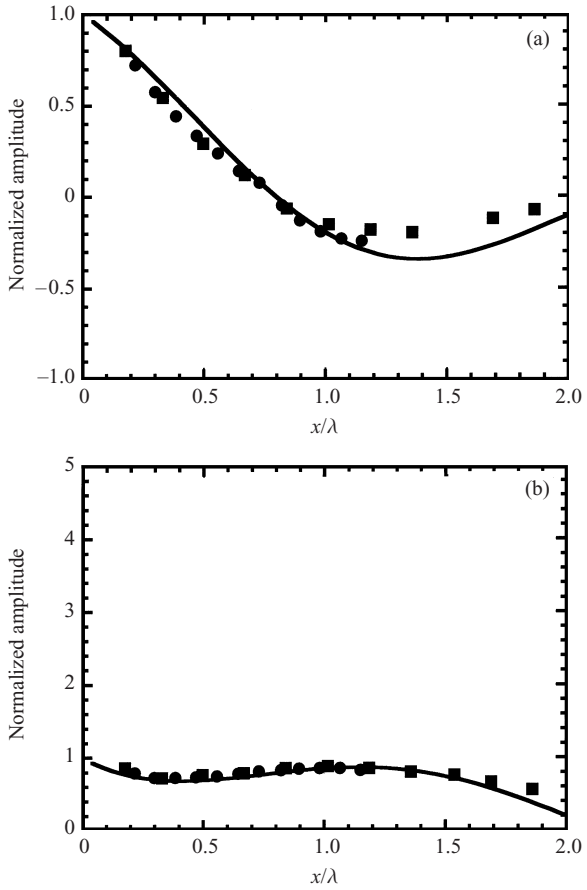

Figure 4. The perturbed amplitudes of the shock front (a) and the ablation front (b). The circles ($a/\lambda = 0.05$) and squares ($a/\lambda = 0.06$) show the simulation results; the curve shows the vertical result. The horizontal and vertical axes are the same as in Fig. 2.

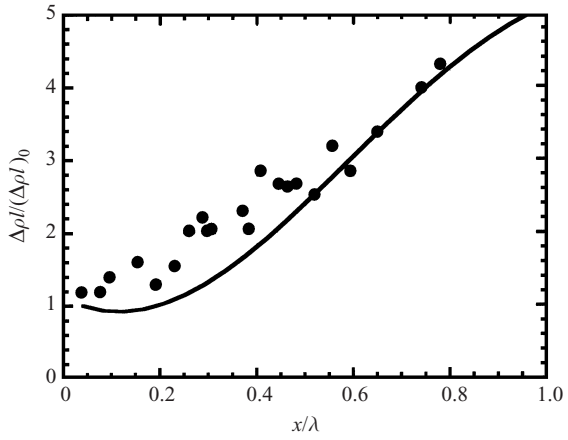

Figure 5. Experimental (circles) and theoretical (curve) results for the perturbed areal mass density. The horizontal and vertical axes are the same as in Fig. 2.

https://doi.org/10.1017/S0022377898007260 Published online by Cambridge University Press

result for the ablation-front ripple agrees well with that of the linear analysis. The restoring-like motion of the ablation front should be noted. Finally, we give a comparison of analytical results with experimental results (Endo et al. 1995) related to the temporal evolution of the perturbed areal mass density, which is done by using the relation $\Delta(\rho l)(t) = \Delta\rho_1(t)\, v_s t + \rho_1\, \Delta l(t)$. It can be seen from Fig. 5 that the analytical curve agrees well with the experimental data points.

5. Concluding remarks

We have investigated the decaying oscillations of the shock-front ripple and the ripple dynamics on the ablation front by linear analysis and simulations. In the linear analysis, the behaviour of the rippled shock is very sensitive to the specific-heat ratio and to the ablation-pressure perturbation on the ablation-front ripple. In the case of $\alpha = 2$ and $\gamma = \frac{5}{3}$ for $\lambda = 100\,\mu$m, the analytical results agree very well with the simulation results. In particular, we have found that growth of the ablation-front ripple *does not* occur in either the linear analysis or the simulation. This is because the ripple amplitude on the ablation front is suppressed by the fire-polishing effect of the ablation surface. The results have been compared with those of recent experiments (Endo et al. 1995). Qualitatively, our analysis explains well the experimental results, as shown in Fig. 5. To sum up, the simple boundary model (2) for the ablation surface can reproduce well the simulation and experimental results for the ablation-front ripple.

Future work will be devoted to taking account of fluid viscosity and also to the analysis of a radiation fluid coupled with equation-of-state effects.

Acknowledgements

We are grateful for theoretical assistance from Dr R. Ishizaki and Professor K. Nishihara. We thank Dr K. Shigemori, Dr M. Nakai and Dr H. Azechi for many useful discussions. We are also grateful to the technical staff at the Institute of Laser Engineering, Osaka University for computational support on this work.

References

Briscoe, M. G. and Kovitz, A. A. 1968 *J. Fluid Mech.* **31**, 529.

Chandrasekhar, S. 1961 *Hydrodynamic and Hydromagnetic Stability*, Chaps X and XIII. Oxford University Press.

Endo, T., Shigemori, K., Azechi, H., Nishiguchi, A., Mima, K., Sato, M. et al. 1995 *Phys. Rev. Lett.* **74**, 3608.

Ishizaki, R. and Nishihara, K. 1997 *Phys. Rev. Lett.* **78**, 1920.

Ishizaki, R., Nishihara, K., Sakagami, H. and Ueshima, Y. 1996 *Phys. Rev.* **E53**, R5592.

Manheimer, W. M., Colombant, D. G. and Gardner, J. H. 1982 *Phys. Fluids* **25**, 1644.

Meshkov, E. E. 1969 *Fluid Dyn.* **4**, 101.

Munro, D. H. 1989 *Phys. Fluids* **B1**, 134.

Nishiguchi, A. and Yabe, T. 1983 *J. Comput. Phys.* **52**, 390.

Richtmyer, R. D. 1960 *Pure Appl. Maths* **13**, 297.

Rutkevich, I., Zaretsky, E. and Mond, M. 1996 *Proceedings of the 24th European Conference on Laser Interaction with Matter, Madrid, 1996*. Report PM-18 (to be published).

Wouchuk, J. G. and Nishihara, K. 1996 *Phys. Plasmas* **3**, 3761.

Wouchuk, J. G. and Nishihara, K. 1997 *Phys. Plasmas* **4**, 1028.